



LUND UNIVERSITY

Physical bounds and sum rules for high-impedance surfaces

Gustafsson, Mats; Sjöberg, Daniel

Published in:

IEEE Transactions on Antennas and Propagation

DOI:

[10.1109/TAP.2011.2143688](https://doi.org/10.1109/TAP.2011.2143688)

2011

Document Version:

Peer reviewed version (aka post-print)

[Link to publication](#)

Citation for published version (APA):

Gustafsson, M., & Sjöberg, D. (2011). Physical bounds and sum rules for high-impedance surfaces. *IEEE Transactions on Antennas and Propagation*, 59(6), 2196-2204. <https://doi.org/10.1109/TAP.2011.2143688>

Total number of authors:

2

General rights

Unless other specific re-use rights are stated the following general rights apply:

Copyright and moral rights for the publications made accessible in the public portal are retained by the authors and/or other copyright owners and it is a condition of accessing publications that users recognise and abide by the legal requirements associated with these rights.

- Users may download and print one copy of any publication from the public portal for the purpose of private study or research.
- You may not further distribute the material or use it for any profit-making activity or commercial gain
- You may freely distribute the URL identifying the publication in the public portal

Read more about Creative commons licenses: <https://creativecommons.org/licenses/>

Take down policy

If you believe that this document breaches copyright please contact us providing details, and we will remove access to the work immediately and investigate your claim.

LUND UNIVERSITY

PO Box 117
221 00 Lund
+46 46-222 00 00

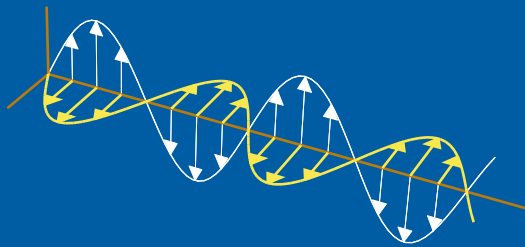
CODEN:LUTEDX/(TEAT-7198)/1-19/(2010)

Revision No. 1: October 2010

Physical bounds and sum rules for high-impedance surfaces

Mats Gustafsson and Daniel Sjöberg

Electromagnetic Theory
Department of Electrical and Information Technology
Lund University
Sweden



Mats Gustafsson and Daniel Sjöberg
Mats.Gustafsson@eit.lth.se, Daniel.Sjoberg@eit.lth.se
Department of Electrical and Information Technology
Electromagnetic Theory
Lund University
P.O. Box 118
SE-221 00 Lund
Sweden

Editor: Gerhard Kristensson
© Mats Gustafsson and Daniel Sjöberg, Lund, October 21, 2010

Abstract

High-impedance surfaces are artificial surfaces synthesized from periodic structures. The high impedance is useful as it does not short circuit electric currents and reflects electric fields without phase shift. Here, a sum rule is presented that relates frequency intervals having high impedance with the thickness of the structure. The sum rule is used to derive physical bounds on the bandwidth for high-impedance surfaces composed by periodic structures above a perfectly conducting ground plane. Numerical examples are used to illustrate the result, and show that the physical bounds are tight.

1 Introduction

A perfect magnetic conductor (PMC) surface is an ideal high-impedance surface. It has infinite impedance meaning that the mirror currents of horizontal electrical currents are not phase shifted. This is desired for low profile antennas as ordinary planar antenna elements can be put on top of a PMC without loss of performance [20, 21]. However, PMCs are artificial surfaces typically synthesized from periodic structures above an ordinary ground plane [20–22]. The properties of the artificial high-impedance surface depend on frequency, polarization, and angle of incidence, and they have high impedance only over finite frequency bands [20, 21].

Here, we introduce a sum rule that relates frequency intervals having impedance above an arbitrary threshold with the static properties of the structure. The sum rule is valid for periodic structures composed by arbitrary dielectric and magnetic materials above a perfect conductor. The sum rule is used to derive physical bounds for high-impedance surfaces. The bounds show how the bandwidth of the high-impedance surface depends on thickness, angle of incidence, polarization, and material properties. The derivation is based on a general approach where integral identities for positive real (PR) functions (or similarly Herglotz functions) are used to construct sum rules [1]. Analogous bounds are used for broadband matching [4], radar absorbers [18], scattering and absorption cross sections [25], antenna performance [9], antenna impedance [6], extraordinary transmission [10], transmission blockages [11], and temporal dispersion of metamaterials [8].

Brewitt-Taylor presented two bounds for high-impedance surfaces in [2]. The first is based on circuit approximation whereas the second is similar to [18]. Another contribution is given in [19], although their result is based on an approximation that may break down for large bandwidths. In comparison, the results presented here are solely based on passivity and make no use of circuit approximations. The new bounds are also sharper than the bounds presented in [2]. Moreover, they hold for lossy as well as lossless surfaces (including possible anisotropy) and for obliquely incident fields. Finally, they are based on an identity and it shows that objects modeled as perfect electric conductors contribute with a negative magnetic polarizability that can affect the performance.

This paper is organized as follows. In Sec. 2, the reflection coefficient and the impedance of periodic high-impedance surfaces are presented. The corresponding

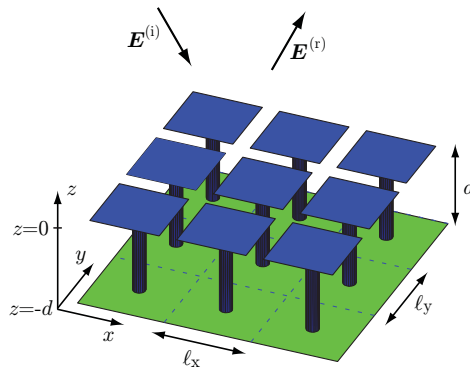


Figure 1: Geometry of a high-impedance surface synthesized by a periodic structure above a perfect conductor.

low-frequency asymptotics are analyzed in Sec. 3. Sum rules and physical bounds are derived in Sec. 4. The bounds are compared with previous results in Sec. 5. Numerical results are presented in Sec. 6.

2 Reflection coefficient and impedance

Consider an infinite array contained in the interval $-d \leq z \leq 0$, with a unit cell Ω lying in the xy -plane and a ground plane at $z = -d$, see Fig. 1. A linearly polarized plane wave impinges on the array in the direction $\hat{\mathbf{k}}$, *i.e.*, $\mathbf{E}^{(i)}(t; \mathbf{r}) = E_0(t - \hat{\mathbf{k}} \cdot \mathbf{r}/c_0) \hat{\mathbf{e}}$ with $\hat{\mathbf{k}} \cdot \hat{\mathbf{z}} < 0$ and $E_0(t') = 0$ for $t' < 0$. Here, $t' = t - \hat{\mathbf{k}} \cdot \mathbf{r}/c_0$, where t is the time variable, c_0 the speed of light in free space, and $\hat{\mathbf{e}}$ the electric polarization of the incident field satisfying $\hat{\mathbf{e}} \cdot \hat{\mathbf{k}} = 0$. The periodicity of the problem implies the translational property

$$\mathbf{E}(t; \mathbf{r} + \mathbf{r}_{mn}) = \mathbf{E}(t - \hat{\mathbf{k}} \cdot \mathbf{r}_{mn}/c_0; \mathbf{r}) \quad (2.1)$$

for all fields, where $\mathbf{r}_{mn} = m\mathbf{a}_1 + n\mathbf{a}_2$ is an arbitrary lattice vector described by two basis vectors \mathbf{a}_1 and \mathbf{a}_2 . The reflected field cannot precede the incident field in $z > 0$, in the meaning that $\mathbf{E}^{(r)}(t; \mathbf{r}) = \mathbf{0}$ if $t < \hat{\mathbf{k}}^{(r)} \cdot \mathbf{r}/c_0$, where $\hat{\mathbf{k}}^{(r)} = \hat{\mathbf{k}} - 2\hat{\mathbf{k}} \cdot \hat{\mathbf{z}}\hat{\mathbf{z}}$ is the mirrored propagation direction. In other words, the reflected field is causal for all $z > 0$ with respect to the incident field, see also [7, 11, 25, 26].

The results in this paper follow from the holomorphic properties of the reflection coefficient and its low- and high-frequency expansions. For this purpose, apply a temporal Laplace transform to the reflected field taking the causality into account by the lower integration limit, *i.e.*,

$$\begin{aligned} \mathbf{E}^{(r)}(\kappa; \mathbf{r}) &= \int_{\hat{\mathbf{k}}^{(r)} \cdot \mathbf{r}/c_0}^{\infty} \mathbf{E}^{(r)}(t; \mathbf{r}) e^{-\kappa t c_0} dt \\ &= e^{-\kappa \hat{\mathbf{k}}^{(r)} \cdot \mathbf{r}} \int_0^{\infty} \mathbf{E}^{(r)}(t' + \hat{\mathbf{k}}^{(r)} \cdot \mathbf{r}/c_0; \mathbf{r}) e^{-\kappa t' c_0} dt' = e^{-\kappa \hat{\mathbf{k}}^{(r)} \cdot \mathbf{r}} \tilde{\mathbf{E}}^{(r)}(\kappa; \mathbf{r}). \end{aligned} \quad (2.2)$$

The field $\tilde{\mathbf{E}}^{(r)}(\kappa; \mathbf{r})$ is Ω -periodic in \mathbf{r} due to the translational property (2.1) and that $\hat{\mathbf{k}}^{(r)}$ has the same xy -components as $\hat{\mathbf{k}}$. The lower integration limit $t' = 0$ for $\tilde{\mathbf{E}}^{(r)}(\kappa; \mathbf{r})$ implies it is holomorphic in the Laplace parameter $\kappa = \sigma + jk$ if this is restricted to the right complex half plane $\text{Re } \kappa \geq 0$, and the imaginary unit is denoted by j . A spectral decomposition in Floquet modes is used outside the array (where the position vector is $\mathbf{r} = x\hat{\mathbf{x}} + y\hat{\mathbf{y}} + z\hat{\mathbf{z}} = \boldsymbol{\rho} + z\hat{\mathbf{z}}$):

$$\tilde{\mathbf{E}}^{(r)}(\kappa; \mathbf{r}) = \sum_{m,n=-\infty}^{\infty} \mathbf{E}_{mn}^{(r)}(k) e^{-j\mathbf{k}_{mn} \cdot \boldsymbol{\rho}} e^{-j(k_{z,mn} - k_{z,00})z}, \quad (2.3)$$

where the expansion coefficients are given by

$$\mathbf{E}_{mn}^{(r)}(\kappa) = \frac{1}{A} \int_{\Omega} \tilde{\mathbf{E}}^{(r)}(k; \mathbf{r}) e^{j\mathbf{k}_{mn} \cdot \boldsymbol{\rho}} e^{j(k_{z,mn} - k_{z,00})z} dS_{\boldsymbol{\rho}}. \quad (2.4)$$

Here, $A = \int_{\Omega} dS$ denotes the area of the unit cell Ω . The reciprocal lattice vectors are defined as $\mathbf{k}_{mn} = m\mathbf{b}_1 + n\mathbf{b}_2$, where the reciprocal basis vectors \mathbf{b}_1 and \mathbf{b}_2 satisfy $\mathbf{a}_i \cdot \mathbf{b}_j = 2\pi\delta_{ij}$ for $i, j = 1, 2$ (δ_{ij} is the Kronecker delta) [14]. Moreover, the wave number in the z -direction is given by $k_{z,mn}^2 = -\kappa^2 + (\kappa\hat{\mathbf{k}}_t + j\mathbf{k}_{mn}) \cdot (\kappa\hat{\mathbf{k}}_t + j\mathbf{k}_{mn})$, where $\hat{\mathbf{k}}_t$ is the transverse part of the unit vector $\hat{\mathbf{k}}$. The transverse components of the expansion coefficients of the reflected field are related to the corresponding expansion coefficients of the incident field via the linear mapping

$$\mathbf{E}_{mn,t}^{(r)}(\kappa) = \sum_{m',n'=-\infty}^{\infty} \boldsymbol{\Gamma}_{mn,m'n'}(\kappa) \cdot \mathbf{E}_{m'n',t}^{(i)}(\kappa). \quad (2.5)$$

The corresponding z -components are given by the requirement that each mode $\mathbf{E}_{mn}^{(i,r)}$ is orthogonal to the total wave vector $-j\kappa\hat{\mathbf{k}}_t + \mathbf{k}_{mn} \pm \hat{\mathbf{z}}k_{z,mn}$. The elements of the 2×2 reflection dyadics $\boldsymbol{\Gamma}_{mn,m'n'}$, are holomorphic functions of κ for $\text{Re } \kappa > 0$ due to causality. It is only a finite number of modes in (2.5) that propagate for a fixed frequency, and, specifically, it is only the lowest order modes ($m = n = m' = n' = 0$) that propagate for frequencies below the first grating lobe [17]. Here, the analysis is restricted to these modes, and the short-hand notation $\Gamma = \hat{\mathbf{e}}_t \cdot \boldsymbol{\Gamma}_{00,00} \cdot \hat{\mathbf{e}}_t / |\hat{\mathbf{e}}_t|^2$ for the co-polarized reflection coefficient is introduced. These are the only modes needed later on, without loss of generality.

Passivity implies that $|\Gamma(\kappa)| \leq 1$ for $\text{Re } \kappa > 0$. The corresponding normalized impedance

$$Z(\kappa) = Z_t \frac{1 + \Gamma(\kappa)}{1 - \Gamma(\kappa)} \quad (2.6)$$

is then a positive real function [5, 28]. The impedance in (2.6) is normalized with respect to the transverse wave impedance $Z_t(\theta) = 1/Y_t(\theta)$, where

$$Y_t(\theta) = \begin{cases} \cos \theta & \text{TE-polarization} \\ 1/\cos \theta & \text{TM-polarization} \end{cases} \quad (2.7)$$

is the transverse wave admittance. The impedance in SI-units is $Z_{\text{SI}} = Z\eta_0$, where $\eta_0 = \sqrt{\mu_0/\epsilon_0} \approx 377 \Omega$ denotes the free-space impedance.

Positive real (related to Herglotz [1] or Nevanlinna) functions are found in the analysis of passive linear systems [5, 28]. They are defined as holomorphic mappings from the right complex half plane into itself and having the real axis mapped into itself. Sum rules, *i.e.*, weighted all spectrum integral identities, are solely determined from the asymptotic expansions of the PR function. In [1], it is shown that the asymptotic expansions

$$P(\kappa) = \sum_{n=0}^{N_0} a_{2n-1} \kappa^{2n-1} + o(\kappa^{2N_0-1}) \quad \text{as } \kappa \hat{\rightarrow} 0 \quad (2.8)$$

and

$$P(\kappa) = \sum_{n=0}^{N_\infty} b_{1-2n} \kappa^{1-2n} + o(\kappa^{1-2N_\infty}) \quad \text{as } \kappa \hat{\rightarrow} \infty \quad (2.9)$$

imply the integral identities

$$\frac{2}{\pi} \int_0^\infty \frac{\text{Re } P(jk)}{k^{2n}} dk = (-1)^{n-1} (a_{2n-1} - b_{2n-1}) \quad (2.10)$$

for $n = 1 - N_\infty, \dots, N_0$. Note that the identity (2.10) should be interpreted as the limit $\lim_{\sigma \rightarrow 0^+} P(\sigma + jk)$, and terms in the right hand side that are not enumerated in (2.8) and (2.9) are zero, see [1]. It is sufficient to have the expansions (2.8) and (2.9) in $|\arg(\kappa)| \leq \pi/2 - \alpha$ for some $\alpha > 0$. It is observed that compositions of PR functions can be used to produce new PR functions and hence sum rules that are particularly suited for an application [1, 8].

3 Low-frequency expansion

3.1 Reflection coefficient

The integral identities (2.10) show that the low- and high-frequency asymptotic expansions can be used to derive constraints on the dynamic properties of the impedance. To determine the low-frequency expansion of the reflection coefficient, we first replace the ground plane with a mirror object in the region $z \in [-2d, -d]$, see Fig. 2. The reflected field is obtained from superposition of the incident field and the mirror field, *i.e.*,

$$\mathbf{E}^{(i)}(\kappa, \mathbf{r}) = E_0 \hat{\mathbf{e}} \exp(-\kappa \hat{\mathbf{k}} \cdot \mathbf{r}) \quad (3.1)$$

$$\mathbf{E}_m^{(i)}(\kappa, \mathbf{r}) = E_0 \hat{\mathbf{e}}^{(r)} \exp(-\kappa \hat{\mathbf{k}}^{(r)} \cdot (\mathbf{r} + 2d\hat{\mathbf{z}})) \quad (3.2)$$

where $\hat{\mathbf{k}}^{(r)} = \hat{\mathbf{k}} - 2\hat{\mathbf{k}} \cdot \hat{\mathbf{z}}\hat{\mathbf{z}}$ and $\hat{\mathbf{e}}^{(r)} = 2\hat{\mathbf{e}} \cdot \hat{\mathbf{z}}\hat{\mathbf{z}} - \hat{\mathbf{e}}$. The reflected field $\mathbf{E}^{(r)}(\kappa, \mathbf{r})$ is obtained as the sum of the reflection of $\mathbf{E}^{(i)}(\kappa, \mathbf{r})$ and the transmission of $\mathbf{E}_m^{(i)}(\kappa, \mathbf{r})$ in the mirrored geometry in Fig. 2b. Using the low-frequency expansion in [23]

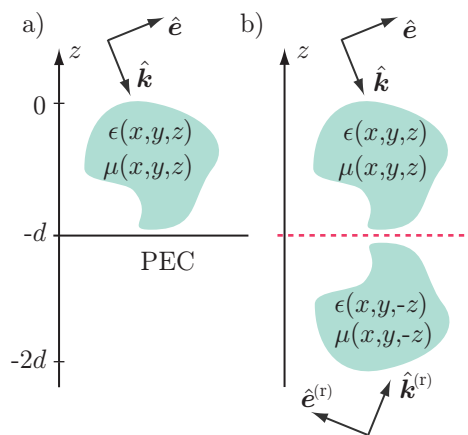


Figure 2: Equivalent problem for the low-frequency expansion. a) original scattering problem with ground plane. b) equivalent scattering problem without the ground plane, where $\hat{\mathbf{k}}^{(r)} = \hat{\mathbf{k}} - 2\hat{\mathbf{k}} \cdot \hat{\mathbf{z}}\hat{\mathbf{z}}$ and $\hat{\mathbf{e}}^{(r)} = 2\hat{\mathbf{e}} \cdot \hat{\mathbf{z}}\hat{\mathbf{z}} - \hat{\mathbf{e}}$.

and that $\mathbf{E}_m^{(i)}(\kappa, \mathbf{r})|_{z=0} = E_0 \hat{\mathbf{e}}^{(r)}(1 - 2\kappa d \cos \theta)$, we derive in the Appendix that the co-polarized reflection coefficient is, to first order in κ ,

$$\Gamma(\kappa) = -1 + \kappa(2d \cos \theta + \gamma/A) + \mathcal{O}(\kappa^2), \quad (3.3)$$

where the polarizability γ is

$$\gamma = \begin{cases} \hat{\mathbf{h}} \cdot \boldsymbol{\gamma}_m \cdot \hat{\mathbf{h}} \cos \theta & \text{TE} \\ \hat{\mathbf{h}} \cdot (\boldsymbol{\gamma}_m + \sin^2 \theta \gamma_e \mathbf{I}) \cdot \hat{\mathbf{h}} \frac{1}{\cos \theta} & \text{TM} \end{cases} \quad (3.4)$$

and the unit vector $\hat{\mathbf{h}} = (\hat{\mathbf{z}} \times \hat{\mathbf{e}})/|\hat{\mathbf{z}} \times \hat{\mathbf{e}}|$ corresponds to the direction of the incident magnetic field in the xy -plane. The magnetic polarizability dyadic $\boldsymbol{\gamma}_m$ is determined in the unit cell Ω subject to periodic boundary conditions in the xy -plane and a magnetostatic field of unit amplitude in the $\hat{\mathbf{h}}$ -direction. More precisely, the magnetic polarizability is defined as

$$\hat{\mathbf{h}} \cdot \boldsymbol{\gamma}_m \cdot \hat{\mathbf{h}} = \hat{\mathbf{h}} \cdot \int_{\Omega \times [-2d, 0]} (\boldsymbol{\mu}_s(\mathbf{r}) - \mathbf{I}) \cdot \mathbf{H}_s(\mathbf{r}) dV, \quad (3.5)$$

where the static field $\mathbf{H}_s(\mathbf{r})$ satisfies the differential equations $\nabla \times \mathbf{H}_s(\mathbf{r}) = \mathbf{0}$ and $\nabla \cdot [\boldsymbol{\mu}_s(\mathbf{r}) \cdot \mathbf{H}_s(\mathbf{r})] = 0$, with mean value $\hat{\mathbf{h}}$ in $\Omega \times (-\infty, \infty)$, or, equivalently, limit values $\mathbf{H}_s(\mathbf{r}) \rightarrow \hat{\mathbf{h}}$ as $z \rightarrow \pm\infty$. Here, $\boldsymbol{\mu}_s(\mathbf{r})$ is the static relative permeability dyadic. We can correspondingly compute an electric polarizability dyadic $\boldsymbol{\gamma}_e$, simply replace $\boldsymbol{\mu}_s$ by $\boldsymbol{\epsilon}_s$. The normal electric polarizability γ_e (a scalar, denoted by γ_{ezz} in the Appendix for clarity) is then computed as

$$\gamma_e = \hat{\mathbf{z}} \cdot \boldsymbol{\gamma}_e \cdot \hat{\mathbf{z}} = \hat{\mathbf{z}} \cdot \int_{\Omega \times [-2d, 0]} (\boldsymbol{\epsilon}_s(\mathbf{r}) - \mathbf{I}) \cdot \mathbf{E}_s(\mathbf{r}) dV, \quad (3.6)$$

where $\mathbf{E}_s(\mathbf{r})$ is the electrostatic solution corresponding to unit excitation in the z direction. For more details on the computation of $\boldsymbol{\gamma}_m$ and $\boldsymbol{\gamma}_e$, in particular when involving PEC structures (where $\mu_s \rightarrow 0$ and $\epsilon_s \rightarrow \infty$), we refer to [23, 24].

3.2 Examples of polarizabilities

The polarizabilities for an isotropic slab (with thickness $2d$ corresponding to the mirrored geometry in Fig. 2) characterized by static relative permeability μ_s and static relative permittivity ϵ_s are

$$\boldsymbol{\gamma}_m = 2Ad(\mu_s - 1)(\hat{\mathbf{x}}\hat{\mathbf{x}} + \hat{\mathbf{y}}\hat{\mathbf{y}}) + 2Ad(1 - \mu_s^{-1})\hat{\mathbf{z}}\hat{\mathbf{z}} \quad (3.7)$$

$$\boldsymbol{\gamma}_e = 2Ad(\epsilon_s - 1)(\hat{\mathbf{x}}\hat{\mathbf{x}} + \hat{\mathbf{y}}\hat{\mathbf{y}}) + 2Ad(1 - \epsilon_s^{-1})\hat{\mathbf{z}}\hat{\mathbf{z}}. \quad (3.8)$$

Using these expressions, we find that (3.4) becomes (using that for TM polarization we can write $\gamma/A = 2d(\mu_s - 1 + \sin^2\theta(1 - \epsilon_s^{-1})) = 2d(\mu_s - \epsilon_s^{-1}\sin^2\theta - \cos^2\theta)$)

$$2d\cos\theta + \gamma/A = \begin{cases} 2d\mu_s\cos\theta & \text{TE} \\ 2d\frac{\mu_s - \epsilon_s^{-1}\sin^2\theta}{\cos\theta} & \text{TM.} \end{cases} \quad (3.9)$$

For normal incidence ($\theta = 0$) we then see that (3.3) becomes

$$\Gamma(\kappa) = -1 + \kappa\mu_s 2d + \mathcal{O}(\kappa^2) \quad (3.10)$$

for both polarizations, which is the familiar result used in [18].

In addition to variations in permittivity and permeability, objects that are modeled as perfect electric conductors (PEC) also give a contribution to the polarizability, in particular $\boldsymbol{\gamma}_m$. These objects can be considered as having static permeability $\mu_r(0) = 0$ and hence have a negative semi-definite $\boldsymbol{\gamma}_m$, *e.g.*, a PEC sphere with radius a has $\boldsymbol{\gamma}_m = -2\pi a^3 \mathbf{I}$. There are a few other shapes with simple expressions for $\boldsymbol{\gamma}_m$ such as spheroids [3]. For a general geometry the polarizabilities can be calculated numerically [15].

Thin patches modeled as PEC are particularly common for high-impedance surfaces [20], see the examples in Sec. 6. They have polarizability dyadics of the form

$$\boldsymbol{\gamma}_m = \gamma_{zz}\hat{\mathbf{z}}\hat{\mathbf{z}} \quad \text{and} \quad \boldsymbol{\gamma}_e = \gamma_{tt}(\hat{\mathbf{x}}\hat{\mathbf{x}} + \hat{\mathbf{y}}\hat{\mathbf{y}}), \quad (3.11)$$

where it is observed that they do not contribute to the low-frequency expansion (3.3). They can however contribute when they are connected to the ground plane with a via. This contribution is analyzed numerically in Sec. 6 but it can also be estimated from the transverse magnetic polarizability of an infinite PEC cylinder of radius a that has

$$\boldsymbol{\gamma}_m = -2\pi a^2 \ell_z (\hat{\mathbf{x}}\hat{\mathbf{x}} + \hat{\mathbf{y}}\hat{\mathbf{y}}) \quad (3.12)$$

per unit length ℓ_z . The electric polarizability along the cylinder grows approximately as ℓ_z^3 , and is increased when the cylinder is terminated by a patch, whereas the magnetic transverse polarizability does not change much by the addition of the patch. The addition of patches improves the approximation of the magnetic polarizability by the infinite cylinder, since the boundary condition $\hat{\mathbf{n}} \cdot \mathbf{H} = 0$ helps keeping the magnetic field in the xy -plane and reduces the fringe field.

Variational results for static problems state that the polarizability dyadics $\boldsymbol{\gamma}_m$ and $\boldsymbol{\gamma}_e$ are monotone in $\boldsymbol{\mu}_s$ and $\boldsymbol{\epsilon}_s$, in the respect that if $\boldsymbol{\mu}_s$ (or $\boldsymbol{\epsilon}_s$) is increased

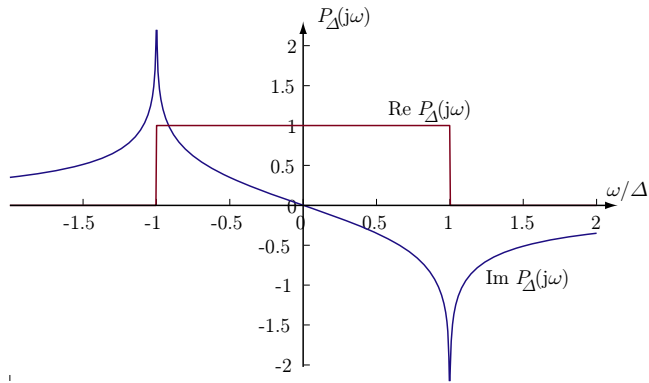


Figure 3: The PR pulse function $P_{\Delta}(j\omega)$ in (4.3).

anywhere in $\Omega \times [-2d, 0]$, then the quadratic form $\hat{\mathbf{h}} \cdot \boldsymbol{\gamma}_m \cdot \hat{\mathbf{h}}$ (or $\hat{\mathbf{z}} \cdot \boldsymbol{\gamma}_e \cdot \hat{\mathbf{z}}$) does not decrease [12, 24]. This means that $\boldsymbol{\gamma}_m$ can be estimated by first increasing $\boldsymbol{\mu}_s$ everywhere up to its maximum value $\max_r \hat{\mathbf{h}} \cdot \boldsymbol{\mu}_s \cdot \hat{\mathbf{h}} = \mu_s^{\max}$. The resulting structure is a homogeneous slab with transverse polarizability $2Ad(\mu_s^{\max} - 1)$ according to (3.7), which is an upper bound to $\hat{\mathbf{h}} \cdot \boldsymbol{\gamma}_m \cdot \hat{\mathbf{h}}$. The normal electric polarizability is estimated by letting $\epsilon_s \rightarrow \infty$ in (3.8), which implies $\gamma_e \leq 2Ad$. Our final estimate is then

$$2d \cos \theta + \gamma/A \leq 2d\mu_s^{\max} Y_t(\theta), \quad (3.13)$$

where $Y_t(\theta)$ is the normalized transverse wave admittance in free space (2.7). This estimate is valid regardless of how the structure is realized, *i.e.*, this bound applies to any structure with thickness d backed by a ground plane, including anisotropic materials and PEC structures.

4 Sum rules and physical bounds

The normalized impedance (2.6) has the low-frequency expansion

$$\frac{Z(\kappa)}{Z_t(\theta)} = \frac{1 + \Gamma(\kappa)}{1 - \Gamma(\kappa)} = \kappa(d \cos \theta + \gamma/(2A)) + \mathcal{O}(\kappa^2) \quad (4.1)$$

as $\kappa \hat{\rightarrow} 0$. We are interested in regions with $\Gamma \approx 1$ or equivalently $|Z| \geq \Delta^{-1}$ where $0 < \Delta < 1$ is a number used to quantify the high-impedance surface. It is also convenient to consider the normalized admittance $Y = 1/Z$ that has $|Y| \leq \Delta$ for high impedance surfaces. The admittance has the asymptotic expansions

$$Y(\kappa) = \begin{cases} \frac{Y_t(\theta)}{\kappa(d \cos \theta + \gamma/(2A))} + o(\kappa^{-1}) & \text{as } \kappa \hat{\rightarrow} 0 \\ \kappa\alpha & \text{as } \kappa \hat{\rightarrow} \infty, \end{cases} \quad (4.2)$$

where $\alpha \geq 0$. The constant α is in general unknown but it is known that the high-frequency asymptotic is at most linear for PR functions [28].

To relate the intervals with $|Y(k)| \leq \Delta$ with the low-frequency asymptotic expansion (4.2), we consider the composition of Y with

$$P_{\Delta}(s) = \frac{1}{\pi} \int_{-\Delta}^{\Delta} \frac{s}{\xi^2 + s^2} d\xi = \frac{1}{j\pi} \ln \frac{js - \Delta}{js + \Delta}. \quad (4.3)$$

that can be extended to the imaginary axis except for $s = \pm j\Delta$, see Fig. 3. This is a positive real function with the properties [8]

$$\begin{cases} \operatorname{Re} P_{\Delta}(s) \leq 1 & \text{for all } s \\ \operatorname{Re} P_{\Delta}(s) \geq 1/2 & \text{for } |s| < \Delta \\ \operatorname{Re} P_{\Delta}(s) = 1 & \text{for } |s| < \Delta \text{ and } \operatorname{Re} s = 0 \\ \operatorname{Re} P_{\Delta}(s) = 0 & \text{for } |s| > \Delta \text{ and } \operatorname{Re} s = 0 \end{cases} \quad (4.4)$$

it is hence well suited to bound regions with low admittance. The composition $P_{\Delta}(Y)$ defines a positive real function with the asymptotic expansions

$$P_{\Delta}(Y(\kappa)) = \begin{cases} \frac{2\kappa(d \cos \theta + \gamma/(2A))\Delta}{\pi Y_t(\theta)} + o(\kappa) & \text{as } \kappa \hat{\rightarrow} 0 \\ o(\kappa) & \text{as } \kappa \hat{\rightarrow} \infty. \end{cases} \quad (4.5)$$

The integral identities for PR function (2.10) gives the $n = 1$ sum rule

$$\int_0^{\infty} \frac{\operatorname{Re} P_{\Delta}(Y(jk))}{k^2} dk = \left(d \cos \theta + \frac{\gamma}{2A} \right) \frac{\Delta}{Y_t(\theta)}. \quad (4.6)$$

Note the sum rule only depends on the low frequency limit due to the $o(\kappa)$ high frequency dependence of $P_{\Delta}(Y(\kappa))$. It is convenient to rewrite it into

$$\int_0^{\infty} \operatorname{Re} P_{\Delta}(Y(\lambda)) d\lambda = \left(d \cos \theta + \frac{\gamma}{2A} \right) \frac{2\pi\Delta}{Y_t(\theta)}, \quad (4.7)$$

where $\lambda = 2\pi/k$ denotes the wavelength and the symbol Y is reused to denote the admittance as function of the wavelength.

Use that the integrand is non-negative to bound (4.7) as

$$B \min_{\lambda \in \mathcal{B}} \operatorname{Re} P_{\Delta}(Y(\lambda)) \leq \frac{1}{\lambda_0} \int_{\lambda_1}^{\lambda_2} \operatorname{Re} P_{\Delta}(Y(\lambda)) d\lambda \leq \frac{2\pi \left(d \cos \theta + \frac{\gamma}{2A} \right) \Delta}{\lambda_0 Y_t(\theta)}, \quad (4.8)$$

where $\mathcal{B} = [\lambda_1, \lambda_2]$, $\lambda_0 = (\lambda_1 + \lambda_2)/2$ is the center wavelength and $B = (\lambda_2 - \lambda_1)/\lambda_0$ is the fractional bandwidth. The properties (4.4) show that $\min_{\lambda \in \mathcal{B}} \operatorname{Re} P_{\Delta}(Y(\lambda)) \geq 1/2$ for $\max_{\lambda \in \mathcal{B}} |Y(\lambda)| = \Delta$ and $\min_{\lambda \in \mathcal{B}} \operatorname{Re} P_{\Delta}(Y(\lambda)) \geq 1$ if in addition $\max_{\lambda \in \mathcal{B}} \operatorname{Re} Y(\lambda) = 0$. Normalizing with λ_0/d , this gives the bound

$$\frac{B\lambda_0}{d} \leq \frac{4\pi}{Y_t(\theta)} \left(\cos \theta + \frac{\gamma}{2Ad} \right) \max_{\lambda \in \mathcal{B}} |Y(\lambda)| \begin{cases} 1 & \text{lossy case} \\ \frac{1}{2} & \text{lossless case} \end{cases} \quad (4.9)$$

which is our main result. The variational bound (3.13) can be used to give

$$\frac{B\lambda_0}{d} \leq 4\pi\mu_s^{\max} \max_{\lambda \in \mathcal{B}} |Y(\lambda)| \begin{cases} 1 & \text{lossy case} \\ 1/2 & \text{lossless case.} \end{cases} \quad (4.10)$$

This version of the bound is independent of the specific realization of the high impedance surface, whereas (4.9) is sharper if the polarizability γ can be computed. A common case is when the high-impedance surface is realized by lossless, non-magnetic materials and operating below the first grating lobe. Allowing $\max_{\lambda \in \mathcal{B}} |Y(\lambda)| = 1/2$, the normalized bandwidth is bounded by

$$\frac{B\lambda_0}{d} \leq \pi. \quad (4.11)$$

In terms of the wavenumber, this becomes $B \leq k_0 d/2$. Note that (4.10) and (4.11) are independent of the angle of incidence.

5 Comparison with previous bounds

The new bound (4.10) is sharper than the bounds presented in [2, 19]. The bounds in [2] are for lossless structures and expressed in the fractional bandwidth B for phase interval Φ , *i.e.*, the reflection has the phase shift $|\phi| \leq \Phi/2$. The ideal high impedance surface has $\phi = 0$. The reflection coefficient has unit amplitude for lossless structures and can be written $\Gamma = e^{-j\phi}$. The corresponding admittance is $Y_{\text{lossless}} = -j \tan(\phi/2)$ with maximum amplitude $\tan(\Phi/4)$ if $\Phi < 2\pi$, giving the bound

$$\frac{B\lambda_0}{d} \leq 2\pi \tan(\Phi/4) \approx \begin{cases} \frac{\pi}{2}\Phi, & \Phi \ll 1 \\ 2\pi, & \Phi = \pi \\ 2.6, & \Phi = \pi/2 \end{cases} \quad (5.1)$$

for normally incident waves. Brewitt-Taylor [2] has

$$\frac{B\lambda_0}{d} \leq \pi\Phi \quad \text{and} \quad \frac{B\lambda_0}{d} \leq \frac{\pi^2}{\ln(2/\Phi)}. \quad (5.2)$$

The first bound is based on a circuit approximation whereas the second uses Cauchy integrals as in [18]. It is noted that the new bound (5.1) is sharper than the bounds in (5.2). The bound in [19] is based on a transmission line model for a frequency selective surface above a ground plane. For a vacuum layer it gives

$$\frac{B\lambda_0}{d} \leq \frac{\pi\Phi \sin^2(kd)}{(kd)^2} \approx \pi\Phi \quad \text{for } kd \ll 1 \quad (5.3)$$

which is similar to (5.2). Once again, the bound (5.1) is tighter.

6 Numerical examples

6.1 Dielectric slab

The reflection coefficient for a normally incident wave on a dielectric slab above a ground plane is

$$\Gamma(\kappa) = \frac{\Gamma_0 - e^{-2\kappa nd}}{1 - \Gamma_0 e^{-2\kappa nd}}, \quad (6.1)$$

where $\kappa = jk + \sigma$, $\Gamma_0 = (\eta - \eta_0)/(\eta + \eta_0)$, $\kappa n = \sqrt{\kappa^2 \epsilon_r}$, and $\eta = 1/\sqrt{\epsilon}$. It has the low frequency expansion

$$\Gamma = -1 + 2\kappa d + \mathcal{O}(\kappa^2), \quad \text{as } \kappa \rightarrow 0. \quad (6.2)$$

As an example, consider the reflection determined in free space at the distance d from a ground plane, *i.e.*, $\epsilon_s = 1$ in the equations above. The admittance is infinite for $d/\lambda = kd/(2\pi) = n/2$ and vanishes for $d/\lambda = 1/4 + n/2$, where $n = 0, 1, 2, \dots$, see Fig. 4. The structure is lossless so the admittance is purely imaginary where it is defined. This means that $\text{Re}\{Y(k)\} = 0$ except at the singular points. The composition $P_\Delta(Y(k))$ is determined for $\Delta = 1/2$, and it is noted that $P_\Delta(Y(k)) = 1$ for wavenumbers such that $|Y(k)| < \Delta = 1/2$.

The sum rule (4.7) shows that the area under the curve $\text{Re} P_\Delta(Y)$ in Fig. 4b is $2\pi\Delta = \pi$. This is also confirmed by numerical integration. The physical bound (4.10) can hence be interpreted as a bound on the area under the curve around the resonance wavelength λ_0 . It is found that $B \approx 59\%$ and $B\lambda_0/d \approx 2.6$. This means that the design is $B/B_{\text{bound}} \approx 2.6/\pi \approx 82\%$ relative an optimal design. The optimal design must have negligible contributions to the area in (4.7) from wavelengths outside the desired resonance.

An increased permittivity, ϵ_r , in the dielectric layer reduces the thickness of the high impedance surface. The functions $\text{Re} P_\Delta(Y)$ and $\text{Im} Y$ are depicted in Fig. 5 for $\epsilon_r = 4$. The bandwidth is determined to $B \approx 31\%$ that is compared to the bound $B_{\text{bound}} \approx 38\%$. Note that $B/B_{\text{bound}} \approx 82\%$ and $B\lambda_0/d \approx 2.6$ are similar to the $\epsilon_r = 1$ case in Fig. 4.

6.2 Mushroom surface

The mushroom structure [20] is one of the most common structures in high impedance surfaces. The structure used here consists of rectangular patches with widths $w_x = w_y = w$ connected to a ground plane by a cylinder with height $d = 8$ mm and radius $a = 1$ mm. The elements are arranged in a rectangular periodic structure with inter-element spacing $\ell = 10$ mm, see Fig. 6. The simulations were made for an infinite PEC periodic structure using the F-solver in the commercial program CST Microwave Studio.

The normalized admittance Y and the composition $P_\Delta(Y)$ are depicted in Fig. 7 as a function of the wavelength for the case $w = 8$ mm. The first grating lobe is at $\lambda/d = 5/4$ meaning that the admittance is purely imaginary for longer wavelengths. It is observed that the admittance $Y \approx 0$ for $\lambda/d \approx 6.9$. In particular it is found that

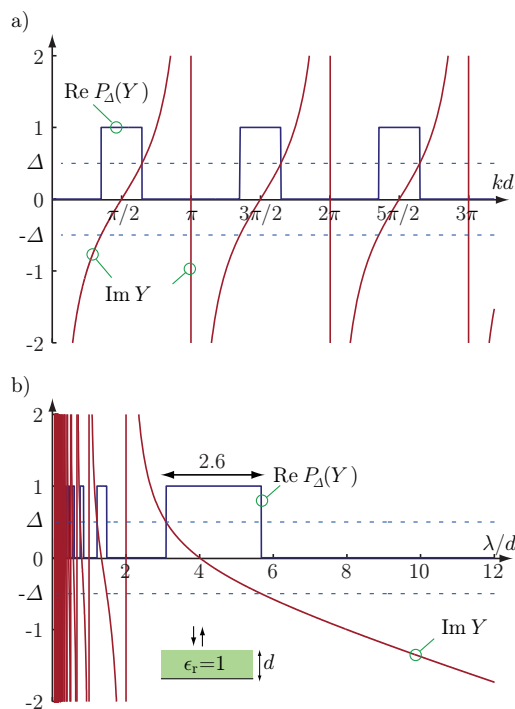


Figure 4: Admittance Y and composition $P_{\Delta}(Y)$ with $\Delta = 1/2$ for the reflection of a dielectric layer with $\epsilon_r = 1$ and thickness d above a ground plane. The normalized center wavelength $\lambda_0/d \approx 4$, normalized bandwidth $B\lambda_0/d \approx 2.6$, bandwidth $B \approx 59\%$ and bound $B/B_{\text{bound}} \approx 82\%$.

$|Y| \leq 1/2$ for $5.5 \leq \lambda/d \leq 8.3$. This gives the normalized bandwidth $B\lambda_0/d \approx 2.8$ that is compared to the upper bound (4.10), *i.e.*, $B\lambda_0/d \leq \pi$, giving the ratio 91%.

An increased coupling between the patches lowers the resonance frequency. The case with $w = 9$ mm is depicted in Fig. 8. It is observed that the normalized bandwidth $B\lambda_0/d \approx 2.9$ that gives the performance $2.9/\pi \approx 92\%$.

The difference between the performance and the upper bound (4.10) can be explained by the magnetic polarizability of the PEC structure. Taking this into account, the corresponding bound would be $B\lambda_0/d \leq \pi(1 + \gamma_m/(2Ad))$. A numerical calculation using the commercial program Comsol Multiphysics shows that $\gamma_m/(2Ad) \approx -0.077$ for $w = 8$ mm and $\gamma_m/(2Ad) \approx -0.081$ for $w = 9$ mm. Note that the simple estimate (3.12) from the polarizability of an infinite cylinder gives the result $\gamma_m/(2Ad) \approx -2\pi a^2/\ell^2 \approx -0.063$, where cylinder radius $a = 1$ mm, cylinder height $\ell_z = 2d = 16$ mm, and unit cell side $\ell = 10$ mm are used.

6.3 Patch surface

In Sec. 6.2 it is observed that the mushroom structure performs close to the physical bound. The difference from the bound is due to the negative contribution of the magnetic polarizability from the cylindrical vias that connect the patches to

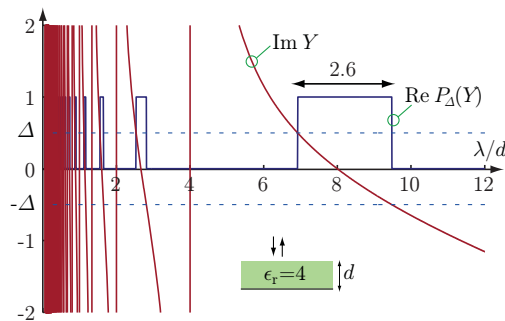


Figure 5: Admittance function Y and composition $P_{\Delta}(Y)$ with $\Delta = 1/2$ for the reflection of a dielectric slab with $\epsilon_r = 4$ and thickness d above a ground plane. The normalized center wavelength $\lambda_0/d \approx 8$, normalized bandwidth $B\lambda_0/2 \approx 2.6$, bandwidth $B \approx 31\%$ and bound $B/B_{\text{bound}} \approx 82\%$.

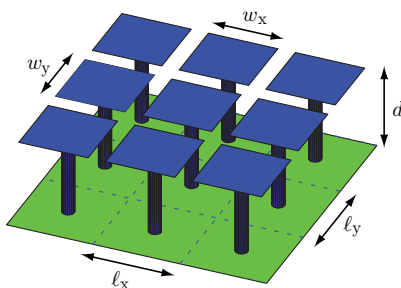


Figure 6: Geometry of the mushroom structure: height d , unit cell $\ell = \ell_x = \ell_y$, and patch width $w = w_x = w_y$.

the ground plane. In the patch surface the vias are removed from the mushroom structure. This creates a structure that should perform close to the physical bound. Note, that the vias are essential for the stop band of the surface wave [13, 20, 21].

The patch structure in Fig. 9 with $w = 9$ mm has the normalized bandwidth $B\lambda_0/d \approx 3.1$ that gives the performance $B/B_{\text{bound}} \approx 98\%$. This confirms that the magnetic polarizability of the PEC vias reduce the performance for the mushroom structure. The performance of the patch structure is further improved with wider patches. The case with $w = 9.9$ mm gives *e.g.*, $\lambda_0/d \approx 10.6$, and the normalized bandwidth $B\lambda_0/d \approx 3.12$ with the performance $B/B_{\text{bound}} \approx 99\%$.

6.4 Oblique incidence

The high-impedance surfaces composed by the dielectric slabs in Sec. 6.1, the mushroom structure in Sec. 6.2 with width $w = 0.9\ell$, and the patch structure in Sec. 6.3 with the width $w = 0.9\ell$ are used to illustrate the bandwidth performance for oblique angles of incidence. CST Microwave studio was used to determine the reflection coefficients in the TE- and TM polarizations for $\theta \leq 80^\circ$. The performance

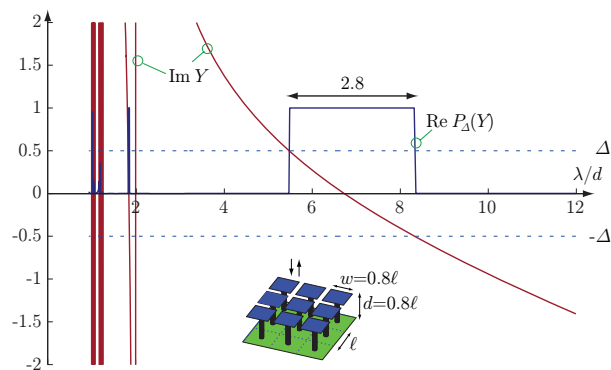


Figure 7: Normalized admittance Y and composition $P_{\Delta}(Y)$ with $\Delta = 1/2$ for a mushroom structure with $\ell = 10$ mm, $w = 8$ mm, and $d = 8$ mm. The normalized center wavelength $\lambda_0/d \approx 6.9$, normalized bandwidth $B\lambda_0/d \approx 2.8$, bandwidth $B \approx 41\%$ and bound $B/B_{\text{bound}} \approx 91\%$.

$B/B_{\text{bound}} = B\lambda_0/(d\pi)$ is depicted in Fig. 10. It is noted that the performance of the patch surface deteriorates for large angles of incidence whereas the mushroom structure performs well, *i.e.*, close to 90%, for all angles of incidence. The performance for the mushroom structure can also be improved by removing the negative magnetic permeability by reducing the radius of the via.

6.5 Aperture surface

Aperture surfaces offer an alternative design for high-impedance surfaces [16]. They are composed of a perforated conducting structure above a ground plane. We use the aperture surface depicted in Fig. 11 to illustrate the sum rule (4.6) and bound (4.10).

The sum rule is evaluated for the metallic part modeled as PEC and with the conductivities $\sigma = 10^5$ S/m and $\sigma = 10^6$ S/m. For the finite conductivities, numerical integration of CST data give values close to $d\pi$ for $\Delta = 1/2$, whereas the PEC integral only gives $0.18d\pi$. It is observed that the integrand in (4.6) approaches the PEC case for $kd > \delta$ for any $\delta > 0$ as $\sigma \rightarrow \infty$, see Fig. 11. However, the integrand also has large contributions from the region $kd \approx 0$ that are not present in the PEC case. The significantly smaller integral for the PEC is due to the extra negative magnetic polarizability for a connected PEC sheet above a ground plane as discussed at the end of the Appendix. This contribution is absent for finite conductivity.

Conclusions

Performance bounds are important as they indicate what is impossible and what might be possible. They also show tradeoffs between different design parameters. Here, a general approach for deriving sum rules and physical bounds on passive systems is utilized to analyze high-impedance surfaces. The bounds show that the

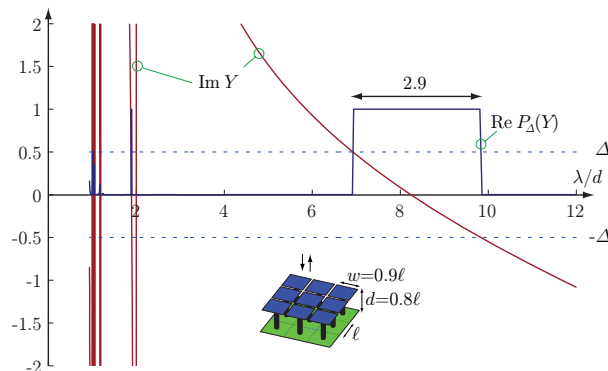


Figure 8: Normalized admittance Y and composition $P_{\Delta}(Y)$ with $\Delta = 1/2$ for a mushroom structure with $\ell = 10$ mm, $w = 9$ mm, and $d = 8$ mm. The normalized center wavelength $\lambda_0/d \approx 8.4$, normalized bandwidth $B\lambda_0/d \approx 2.9$, bandwidth $B = 34\%$ and bound $B/B_{\text{bound}} \approx 92\%$.

bandwidth depends on the thickness and the static permeability for normally incident waves. There is also a contribution from the polarizability dyadics for oblique angles of incidence and material structures modeled as PEC.

7 Acknowledgement

The authors gratefully acknowledges the financial support of the Swedish Research Council (VR), the Swedish Foundation of Strategic Research (SSF), and the Swedish Defence Materiel Administration (FMV).

Appendix A Low-frequency expansion

In this appendix, we calculate the low frequency reflection from a general structure with a ground plane as in Fig. 1. By using the mirror field as described in Fig. 2, the transverse reflected field can be expressed as (where index t denotes transverse components)

$$\mathbf{E}_t^{(r)}(\kappa, \mathbf{r}) = \left(\mathbf{r} \cdot \mathbf{E}_t^{(i)}(\kappa, \mathbf{r}) + \mathbf{t} \cdot \mathbf{E}_{m,t}^{(i)}(\kappa, \mathbf{r}) \right) |_{z=0} e^{-\kappa \hat{\mathbf{k}}^{(r)} \cdot \mathbf{r}} \quad (\text{A.1})$$

The matrices \mathbf{r} and \mathbf{t} are the transverse reflection and transmission matrices for a low-pass structure (without a ground plane, corresponding to Fig. 2b) as described in [23]. The mirror symmetry in Fig. 2 implies that an exciting field in the z direction can not cause a total electric or magnetic dipole moment in the transverse direction, and *vice versa*. The low-frequency expansions in [23] of these matrices are then (up to first order in κ , where $\hat{\mathbf{k}}_t$ is the transverse part of the propagation direction $\hat{\mathbf{k}}$

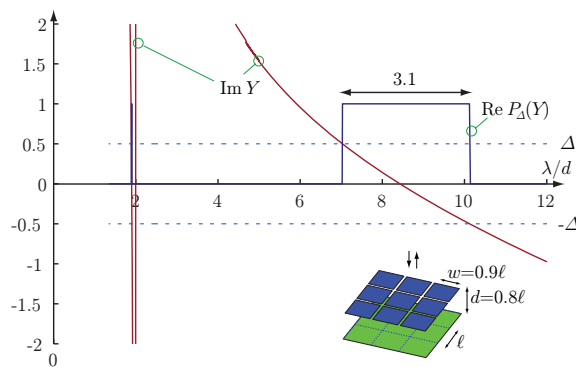


Figure 9: Normalized admittance Y and composition $P_{\Delta}(Y)$ with $\Delta = 1/2$ for a patch structure with $\ell = 10$ mm, $w = 9$ mm, and $d = 8$ mm. The normalized center wavelength $\lambda_0/d \approx 8.6$, normalized bandwidth $B\lambda_0/d \approx 3.1$, bandwidth $B \approx 36\%$ and bound $B/B_{\text{bound}} \approx 98\%$.

and $\hat{\mathbf{k}}'_t = \hat{\mathbf{z}} \times \hat{\mathbf{k}}_t$)

$$\mathbf{r}(\kappa) = -\frac{\kappa}{2} \left\{ \mathbf{Z}_0 \cdot \left[\frac{\gamma_{\text{ett}}}{A} + \frac{\hat{\mathbf{k}}'_t \hat{\mathbf{k}}'_t \gamma_{\text{mzz}}}{A} \right] - \left[-\hat{\mathbf{z}} \times \frac{\gamma_{\text{mtt}}}{A} \cdot \hat{\mathbf{z}} \times + \hat{\mathbf{k}}_t \hat{\mathbf{k}}_t \frac{\gamma_{\text{ezz}}}{A} \right] \cdot \mathbf{Z}_0^{-1} \right\} \quad (\text{A.2})$$

and

$$\mathbf{t}(\kappa) = \mathbf{I} - \frac{\kappa}{2} \left\{ \mathbf{Z}_0 \cdot \left[\frac{\gamma_{\text{ett}}}{A} + \frac{\hat{\mathbf{k}}'_t \hat{\mathbf{k}}'_t \gamma_{\text{mzz}}}{A} \right] + \left[-\hat{\mathbf{z}} \times \frac{\gamma_{\text{mtt}}}{A} \cdot \hat{\mathbf{z}} \times + \hat{\mathbf{k}}_t \hat{\mathbf{k}}_t \frac{\gamma_{\text{ezz}}}{A} \right] \cdot \mathbf{Z}_0^{-1} \right\} \quad (\text{A.3})$$

The normalized wave impedance dyadic in free space is

$$\mathbf{Z}_0 = \cos \theta \frac{\hat{\mathbf{k}}_t \hat{\mathbf{k}}_t}{|\hat{\mathbf{k}}_t|^2} + \frac{1}{\cos \theta} \frac{\hat{\mathbf{k}}'_t \hat{\mathbf{k}}'_t}{|\hat{\mathbf{k}}_t|^2} \quad (\text{A.4})$$

The electric and magnetic polarizability matrices γ_e and γ_m are defined by the induced electric and magnetic dipole moments $\mathbf{p} = \epsilon_0 \gamma_e \cdot \mathbf{E}_0$ and $\mathbf{m} = \gamma_m \cdot \mathbf{H}_0$ for applied static fields \mathbf{E}_0 and \mathbf{H}_0 . They are decomposed in transverse and longitudinal parts as

$$\gamma_e = \gamma_{\text{ett}} + \gamma_{\text{etz}} \hat{\mathbf{z}} + \hat{\mathbf{z}} \gamma_{\text{ezt}} + \gamma_{\text{ezz}} \hat{\mathbf{z}} \hat{\mathbf{z}} \quad (\text{A.5})$$

The dyadic γ_{ett} has only transverse components and can be represented as a 2×2 matrix, γ_{etz} and γ_{ezt} are vectors in the transverse plane, and γ_{ezz} is a scalar. Corresponding expressions apply for γ_m . The co-polarized reflection coefficient $\Gamma(\kappa)$ is then

$$\Gamma(\kappa) = \frac{\hat{\mathbf{e}}_t \cdot \mathbf{r}(\kappa) \cdot \hat{\mathbf{e}}_t + \hat{\mathbf{e}}_t \cdot \mathbf{t}(\kappa) \cdot \hat{\mathbf{e}}_t^{(r)} e^{-\kappa 2d \cos \theta}}{|\hat{\mathbf{e}}_t|^2} \quad (\text{A.6})$$

where $\hat{\mathbf{e}}_t$ is the transverse part (xy -components) of the polarization vector $\hat{\mathbf{e}}$, with the mirror polarization satisfying $\hat{\mathbf{e}}_t^{(r)} = -\hat{\mathbf{e}}_t$. The exponential factor $e^{-\kappa 2d \cos \theta}$ is due

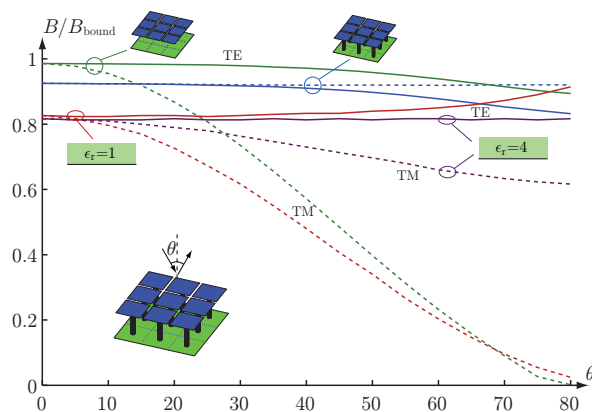


Figure 10: Performance $B/B_{\text{bound}} = B\lambda_0/(d\pi)$ for dielectric slabs and the mushroom and patch structures with $w = 0.9\ell$ as functions of the angle of incidence θ .

to $\mathbf{E}_m^{(i)}(\kappa, \mathbf{r})|_{z=0} = E_0 \hat{\mathbf{e}}^{(r)} e^{-\kappa 2d \hat{\mathbf{k}}^{(r)} \cdot \hat{\mathbf{z}}}$. To first order in κ , the low frequency expansion is given by

$$\mathbf{r}(\kappa) - \mathbf{t}(\kappa) e^{-\kappa 2d \cos \theta} = -\mathbf{I} + \kappa \left\{ 2d \cos \theta \mathbf{I} + \left[-\hat{\mathbf{z}} \times \frac{\gamma_{\text{mtt}}}{A} \cdot \hat{\mathbf{z}} \times + \hat{\mathbf{k}}_t \hat{\mathbf{k}}_t \frac{\gamma_{\text{ezz}}}{A} \right] \cdot \mathbf{Z}_0^{-1} \right\} \quad (\text{A.7})$$

In TE polarization we have $\hat{\mathbf{e}}_t \sim \hat{\mathbf{k}}_t' \perp \hat{\mathbf{k}}_t$, which implies

$$\Gamma_{\text{TE}}(\kappa) = -1 + \kappa \left\{ 2d \cos \theta + \left(\frac{\hat{\mathbf{z}} \times \hat{\mathbf{e}}_t}{|\hat{\mathbf{e}}_t|} \right) \cdot \frac{\gamma_{\text{mtt}}}{A} \cdot \left(\frac{\hat{\mathbf{z}} \times \hat{\mathbf{e}}_t}{|\hat{\mathbf{e}}_t|} \right) \cos \theta \right\} \quad (\text{A.8})$$

In TM polarization we have $\hat{\mathbf{e}}_t \sim \hat{\mathbf{k}}_t \perp \hat{\mathbf{k}}_t'$, which implies

$$\Gamma_{\text{TM}}(\kappa) = -1 + \kappa \left\{ 2d \cos \theta + \left(\frac{\hat{\mathbf{z}} \times \hat{\mathbf{e}}_t}{|\hat{\mathbf{e}}_t|} \right) \cdot \frac{\gamma_{\text{mtt}} + |\hat{\mathbf{k}}_t|^2 \gamma_{\text{ezz}} \mathbf{I}}{A} \cdot \left(\frac{\hat{\mathbf{z}} \times \hat{\mathbf{e}}_t}{|\hat{\mathbf{e}}_t|} \right) \frac{1}{\cos \theta} \right\} \quad (\text{A.9})$$

We can then write the reflection coefficient as

$$\Gamma(\kappa) = -1 + \kappa(2d \cos \theta + \gamma/A) + \mathcal{O}(\kappa^2) \quad (\text{A.10})$$

where (using that $|\hat{\mathbf{k}}_t| = \sin \theta$)

$$\gamma = \begin{cases} \hat{\mathbf{h}} \cdot \gamma_m \cdot \hat{\mathbf{h}} \cos \theta & \text{TE} \\ \hat{\mathbf{h}} \cdot (\gamma_m + \sin^2 \theta \gamma_e \mathbf{I}) \cdot \hat{\mathbf{h}} \frac{1}{\cos \theta} & \text{TM} \end{cases} \quad (\text{A.11})$$

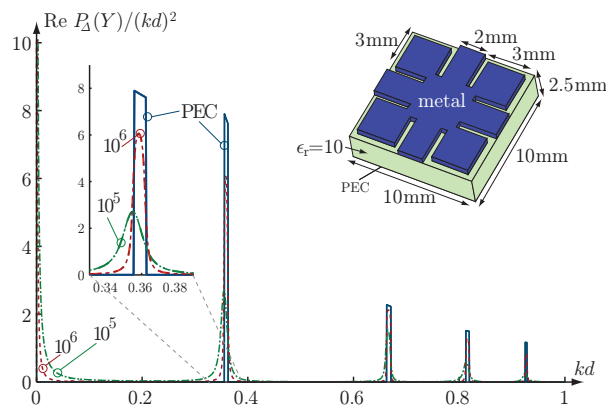


Figure 11: Integrand, $\text{Re}\{P_{\Delta}(Y(kd))\}/(kd)^2$, in (4.6) for periodic aperture high-impedance surfaces with a 0.5 mm metallic layer modeled as PEC, $\sigma = 10^5$ S/m, and $\sigma = 10^6$ S/m. The layer is backed by a 2.5 mm thick $\epsilon_r = 10$ slab and a PEC ground plane.

The vector $\hat{\mathbf{h}} = (\hat{\mathbf{z}} \times \hat{\mathbf{e}}_t)/|\hat{\mathbf{e}}_t|$ has unit length, and since it is in the xy -plane we are able to replace γ_{mtt} by the full matrix γ_{m} to simplify the notation. We also replaced γ_{ezz} by γ_{e} for further simplification.

The low frequency expansion (A.10) is valid also for structures where a static current can flow through the unit cell, for instance a continuous metal surface with apertures. When modeling the metal surface with finite conductivity, the analysis in this Appendix is readily generalized since there can be no static transverse current in the mirrored problem due to the symmetry of excitation. When modeling the metal surface with PEC, a refined analysis shows that the polarizability γ has an additional term, corresponding to the magnetic moment of the mirrored static current. This cancels the term $2d \cos \theta$, leaving only the polarizabilities of the apertures as contributions to the low frequency limit. These polarizabilities are positive and can be calculated using integral equations [27]. This means the low frequency limit is still given by (A.10), but the term $2d \cos \theta + \gamma/A$ is substantially smaller than the corresponding finite conductivity case.

A simple example to demonstrate this behavior is a PEC sheet with distance d to the ground plane, which is mirrored to produce two PEC sheets spaced by $2d$. The incident field generates a surface current $2\hat{\mathbf{z}} \times \mathbf{H}_t^{(i)}$ at the top, and the mirrored incident field generates a surface current $-2\hat{\mathbf{z}} \times \mathbf{H}_t^{(i)}$ on the bottom. Thus, the total transverse current is zero, but there is a magnetic moment $\mathbf{m} = -2dA\mathbf{H}_t^{(i)}$. This means the polarizability is (using that $\gamma_{\text{e}} = 2dA$)

$$\gamma = \begin{cases} -2dA \cos \theta & \text{TE} \\ (-2dA + \sin^2 \theta 2dA) \frac{1}{\cos \theta} = -2dA \cos \theta & \text{TM} \end{cases} \quad (\text{A.12})$$

which implies $2d \cos \theta + \gamma/A = 0$, and hence $\Gamma(\kappa) = -1$, as expected for the reflection from a PEC sheet.

References

- [1] A. Bernland, A. Luger, and M. Gustafsson. Sum rules and constraints on passive systems. Technical Report LUTEDX/(TEAT-7193)/1-31/(2010), Lund University, Department of Electrical and Information Technology, P.O. Box 118, S-221 00 Lund, Sweden, 2010. <http://www.eit.lth.se>.
- [2] C. R. Brewitt-Taylor. Limitation on the bandwidth of artificial perfect magnetic conductor surfaces. *Microwaves, Antennas & Propagation, IET*, **1**(1), 255–260, 2007.
- [3] R. E. Collin. *Field Theory of Guided Waves*. IEEE Press, New York, second edition, 1991.
- [4] R. M. Fano. Theoretical limitations on the broadband matching of arbitrary impedances. *Journal of the Franklin Institute*, **249**(1,2), 57–83 and 139–154, 1950.
- [5] E. A. Guillemin. *The Mathematics of Circuit Analysis*. MIT Press, 1949.
- [6] M. Gustafsson. Sum rules for lossless antennas. *IET Microwaves, Antennas & Propagation*, **4**(4), 501–511, 2010.
- [7] M. Gustafsson. Time-domain approach to the forward scattering sum rule. *Proc. R. Soc. A*, 2010.
- [8] M. Gustafsson and D. Sjöberg. Sum rules and physical bounds on passive metamaterials. *New Journal of Physics*, **12**, 043046, 2010.
- [9] M. Gustafsson, C. Sohl, and G. Kristensson. Illustrations of new physical bounds on linearly polarized antennas. *IEEE Trans. Antennas Propagat.*, **57**(5), 1319–1327, May 2009.
- [10] M. Gustafsson. Sum rule for the transmission cross section of apertures in thin opaque screens. *Opt. Lett.*, **34**(13), 2003–2005, 2009.
- [11] M. Gustafsson, C. Sohl, C. Larsson, and D. Sjöberg. Physical bounds on the all-spectrum transmission through periodic arrays. *EPL Europhysics Letters*, **87**(3), 34002 (6pp), 2009.
- [12] D. S. Jones. Scattering by inhomogeneous dielectric particles. *Quart. J. Mech. Appl. Math.*, **38**, 135–155, 1985.
- [13] P. S. Kildal and A. Kishk. EM modeling of surfaces with STOP or GO characteristics — artificial magnetic conductors and soft and hard surfaces. *Appl. Comput. Electromagn. Soc. J.*, **18**(1), 32–40, March 2003.
- [14] C. Kittel. *Introduction to Solid State Physics*. John Wiley & Sons, New York, 7 edition, 1996.

- [15] R. E. Kleinman and T. B. A. Senior. Rayleigh scattering. In V. V. Varadan and V. K. Varadan, editors, *Low and high frequency asymptotics*, volume 2 of *Handbook on Acoustic, Electromagnetic and Elastic Wave Scattering*, chapter 1, pages 1–70. Elsevier Science Publishers, Amsterdam, 1986.
- [16] K. P. Ma, K. Hirose, F. R. Yang, Y. Qian, and T. Itoh. Realisation of magnetic conducting surface using novel photonic bandgap structure. *Electronics Letters*, **34**(21), 2041–2042, 1998.
- [17] B. Munk. *Frequency Selective Surfaces: Theory and Design*. John Wiley & Sons, New York, 2000.
- [18] K. N. Rozanov. Ultimate thickness to bandwidth ratio of radar absorbers. *IEEE Trans. Antennas Propagat.*, **48**(8), 1230–1234, August 2000.
- [19] M. F. Samani and R. Safian. On bandwidth limitation and operating frequency in artificial magnetic conductors. *IEEE Antennas & Wireless Propagation Letters*, **9**, 228–231, 2010.
- [20] D. Sievenpiper, L. Zhang, R. F. J. Broas, and N. G. Alexopolous. High impedance electromagnetic surfaces with a forbidden frequency band. *IEEE Trans. Microwave Theory Tech.*, **47**(11), 2059–2074, 1999.
- [21] D. F. Sievenpiper. Artificial impedance surfaces for antennas. In C. A. Balanis, editor, *Modern Antenna Handbook*, pages 737–778. Wiley-Interscience, 2008.
- [22] C. R. Simovski, M. E. Ermutlu, A. A. Sochava, and S. A. Tretyakov. Magnetic properties of novel high impedance surfaces. *Microwaves, Antennas & Propagation, IET*, **1**(1), 190–197, 2007.
- [23] D. Sjöberg. Low frequency scattering by passive periodic structures for oblique incidence: low pass case. *J. Phys. A: Math. Theor.*, **42**, 385402, 2009.
- [24] D. Sjöberg. Variational principles for the static electric and magnetic polarizabilities of anisotropic media with perfect electric conductor inclusions. *J. Phys. A: Math. Theor.*, **42**, 335403, 2009.
- [25] C. Sohl, M. Gustafsson, and G. Kristensson. Physical limitations on broadband scattering by heterogeneous obstacles. *J. Phys. A: Math. Theor.*, **40**, 11165–11182, 2007.
- [26] C. Sohl, C. Larsson, M. Gustafsson, and G. Kristensson. A scattering and absorption identity for metamaterials: experimental results and comparison with theory. *J. Appl. Phys.*, **103**(5), 054906, 2008.
- [27] J. van Bladel. *Electromagnetic Fields*. IEEE Press, Piscataway, NJ, second edition, 2007.
- [28] A. H. Zemanian. *Distribution theory and transform analysis: an introduction to generalized functions, with applications*. Dover Publications, New York, 1987.